Citation: Molecular Therapy — Methods & Clinical Development (2014) **1,** 4; doi:10.1038/mtm.2013.4

www.nature.com/mtm

ARTICLE

Differential effects of two MRI contrast agents on the integrity and distribution of rAAV2 and rAAV5 in the rat striatum

Sue Osting[1], Antonette Bennett[2], Shelby Power[1], Jordan Wackett[1], Samuel A Hurley[3], Andrew L Alexander[3–5], Mavis Agbandje-Mckena[2] and Corinna Burger[1]

Intraoperative magnetic resonance imaging (MRI) has been proposed as a method to optimize intracerebral targeting and for tracking infusate distribution in gene therapy trials for nervous system disorders. We thus investigated possible effects of two MRI contrast agents, gadoteridol (Gd) and galbumin (Gab), on the distribution and levels of transgene expression in the rat striatum and their effect on integrity and stability of recombinant adeno-associated virus (rAAV) particles. MRI studies showed that contrast agent distribution did not predict rAAV distribution. However, green fluorescent protein (GFP) immunoreactivity revealed an increase in distribution of rAAV5-GFP, but not rAAV2-GFP, in the presence of Gd when compared with viral vector injected alone. In contrast, Gab increased the distribution of rAAV2-GFP not rAAV5-GFP. These observations pointed to a direct effect of infused contrast agent on the rAAV particles. Negative-stain electron microscopy (EM), DNAase treatment, and differential scanning calorimetry (DSC) were used to monitor rAAV2 and rAAV5 particle integrity and stability following contrast agent incubation. EMs of rAAV2-GFP and rAAV5-GFP particles pretreated with Gd appear morphologically similar to the untreated sample; however, Gab treatment resulted in surface morphology changes and aggregation. A compromise of particle integrity was suggested by sensitivity of the packaged genome to DNAase treatment following Gab incubation but not Gd for both vectors. However, neither agent significantly affected particle stability when analyzed by DSC. An increase in T_m was observed for AAV2 in lactated Ringer's buffer. These results thus highlight potential interactions between MRI contrast agents and AAV that might affect vector distribution and stability, as well as the stabilizing effect of lactated Ringer's solution on AAV2.

Molecular Therapy — Methods & Clinical Development (2014) **1**, 4; doi:10.1038/mtm.2013.4; published online 8 January 2014

INTRODUCTION

One of the challenges of intracerebral delivery is that small differences in targeting affect the distribution of molecules,[1] hindering efficacy, and inducing adverse effects.[2] Careful intraoperative magnetic resonance imaging (MRI) targeting and monitoring of infusate distribution are proposed as methods to optimize treatment delivery. For many years, MRI in combination with intravenous administration of contrast agents, typically based on gadolinium compounds, has been safely used in humans to visualize cerebral blood vessels.[3–5] Due to the fact that free gadolinium is highly toxic (Gd^{3+}; refs. 6–8), chelates of Gd^{3+} have been developed to avoid this effect.[9] In addition, covalent attachment to large proteins, such as albumin to gadolinium, has been used to avoid the fast clearance of the agents, to enhance MRI visualization, and to mimic diffusion properties of particles and drugs of larger molecular weight.[10–12] Typically, the diffusion properties of contrast agents are directly related to the molecular weight of the agent, with higher molecular weight agents diffusing more slowly and over a more limited volume; agents with a molecular weight closely matching that of the infusate may be surrogate markers of distribution volume.[13] Lately, these same contrast agents have been used in experimental and clinical applications as intracerebral infusates to facilitate targeting and visualization of infusions.[14,15]

The clinical efficacy of viral vectors are affected by mis-targeting and overall factors that affect intracerebral distribution of molecules.[1] Therefore, intraoperative MRI combined with coinfusion of viral vectors and contrast agents has been proposed to actively monitor infusate and predict the distribution of the vector and therapeutic transgene in the brain.[16–21] For the recombinant adeno-associated virus (rAAV) vector system, these experiments have been carried out with the AAV1 and AAV2 serotypes,[16–21] and little is known about the behavior of other serotypes or the physical manifestations of the interaction between these vectors and the contrast agents. AAV5 vectors exhibit higher transgene distribution than AAV2 vectors in distinct regions of the brain in different animal models.[22–24] However, most of the completed clinical trials for neurological disorders have used the rAAV2 serotype, mainly because its safety profile has long been proved in many clinical studies.[25–27] Gene therapeutic approaches to treat human neurological disorders require distribution of the transgene in the large human brain,

[1]Department of Neurology, University of Wisconsin, Madison, Wisconsin, USA; [2]Department of Biochemistry, University of Florida, Gainesville, Florida, USA; [3]Department of Medical Physics, University of Wisconsin, Madison, Wisconsin, USA; [4]Department of Psychiatry, University of Wisconsin, Madison, Wisconsin, USA; [5]Waisman Laboratory for Brain Imaging and Behavior, University of Wisconsin, Madison, Wisconsin, USA.
Correspondence: C Burger (burger@neurology.wisc.edu)
The first two authors contributed equally to this work.
Received 24 October 2013; revised; accepted 30 October 2013

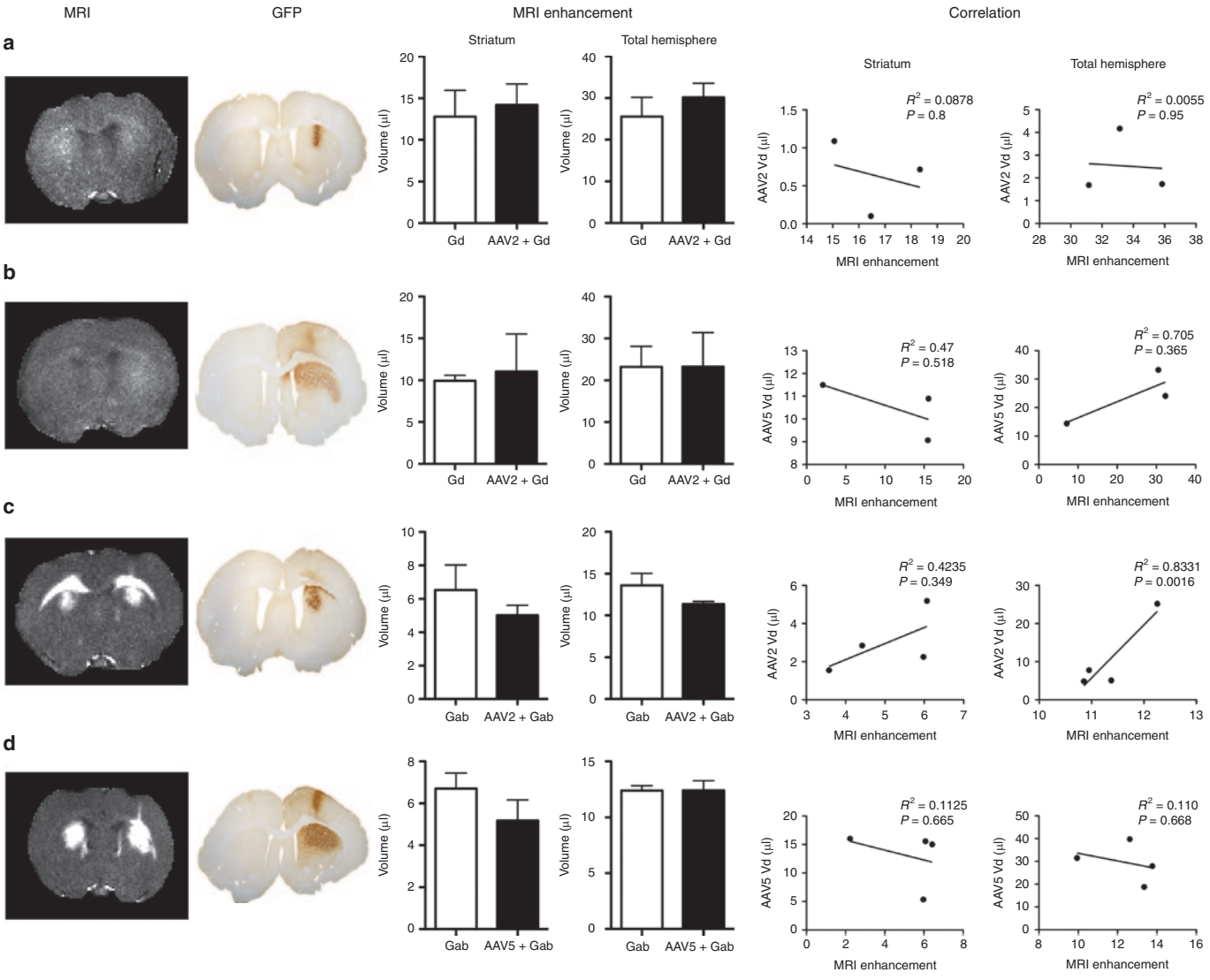

Figure 1 Effects of Gd and Gab on MRI enhancement and GFP distribution of rAAV2 and rAAV5. The first and second columns show the R_1 (=1/T_1) maps from the MRI and the corresponding GFP staining for six animals. Note that the GFP is only visible on the side with the viral vector, while the MRI enhancement is bilateral (only the right hemisphere was injected with rAAV-GFP). The plots labeled "MRI enhancement" compare the the volumes enhanced by contrast infusion with (right hemisphere) and without the viral vector (left hemisphere). No statistically significant differences for MRI enhancement were observed between striatal hemispheres or total brain. The plots labeled "correlation" show Pearson's correlation analysis between the MRI volume of enhancement and the volume of rAAV distribution analyzed for both striatum and total brain. Data expressed as volume ± SEM. $n = 4$ for all experimental groups, except the Gd/AAV5-GFP ($n = 3$; one animal was removed from the analysis due to motion artifact). Scale bar = 1 mm. Gab, galbumin; Gd, gadoteridol; GFP, green fluorescent protein; MRI, magnetic resonance imaging; rAAV, recombinant adeno-associated virus.

where widespread distribution of the viral vector is warranted. Indeed, insufficient spread of the transgene was reported as one of the causes for lack of clinical efficacy in a phase 2 double-blind trial for Parkinson's disease.[28,29] Currently, preclinical studies are being carried out using AAV serotypes that display a more efficient distribution than AAV2 in the central nervous system.[30]

Future gene therapy clinical trials for neurological disorders will likely include coinfusion of MRI contrast agents and rAAV. Since gadolinium has the ability to form complexes with a number of ligands,[31] its coinfusion with viral vectors may affect their transduction efficacy. Due to the potential clinical impact of this coinfusion method, we set out to investigate whether coinfusion of two common MRI imaging compounds, Gd (gadoliniuim complex of 10-(2-hydroxy-propyl)-1,4,7,10-tetraazacyclododecane-1, 4, 7-triacetic acid; Gd) or gadolinium-labeled albumin (galbumin or Gab)[32] with AAV2 or AAV5, affect viral vector distribution and viral particle stability. We were particularly interested to determine whether Gd or Gab spread predicts the actual distribution of these two vectors in the rat striatum. We used electron microscopy (EM), DNAase treatment, and calorimetric studies to analyze the integrity and interaction properties of the two vectors exposed to these contrast agents. These studies showed that different contrast agents have distinct effects on the properties of AAV2 and AAV5.

RESULTS

rAAV2 and rAAV5 show differences in distribution of MRI enhancement and green fluorescent protein expression

It has been shown that the distribution of infused gadolinium-loaded liposomes can predict distribution of rAAV1, but not rAAV2, in the primate brain,[18] although the same group later reported that Gd distribution does predict AAV2 distribution.[19] MRI and histology were used to track the distribution of Gd and Gab in the presence

or absence of viral vector. Animals were injected bilaterally, and each injection consisted of 1 µl of contrast agent and 1 µl of lactated Ringer's solution (left hemisphere) or 1 µl of viral vector and 1 µl of contrast agent (right hemisphere; see Materials and Methods for details). MRI was performed immediately after surgery, with a mean time of 1 hour between the beginning of the first infusion and beginning of imaging. MRI and postmortem immunohistochemical analysis of the tissue (3 weeks post-MRI) were carried out to examine possible correlation between tracer and transgene distribution.

The distribution of contrast agents was visualized and estimated using quantitative R_1 (=1/T_1) relaxometry (Figure 1, left column labeled MRI). Slices of the magnetic resonance examination were taken to match stained histological slices (Figure 1, column labeled GFP), and visual inspection showed similar patterns of MRI signal enhancement both with and without the viral vector. Note that Gab showed much stronger contrast enhancement than Gd on magnetic resonance examinations (given the same quantitative R1 scale), likely due to the slower diffusion of Gab.[33] The regions of enhancement were manually traced. Both striatal signal and total brain hemisphere signal were measured, because it was observed that MRI contrast agents tend to flow up the injection track, as shown in this study and by others,[1] resulting in rAAV distribution in unwanted areas (Figure 1, column labeled GFP). The average distribution volumes of enhancement are plotted in Figure 1 (MRI enhancement) for both striatum and total brain hemisphere. For infusions with both Gd (Figure 1a,b) and Gab (Figure 1c,d), there were no significant enhancement differences whether or not a viral vector was present (Figure 1 (Gd/rAAV2-green fluorescent protein (GFP) striatum, $P = 0.7357$; total brain, $P = 0.4495$; $n = 4$) (Gd/rAAV5-GFP striatum, $P = 0.818$; total brain $P = 0.9945$; $n = 3$) (Gab/rAAV2-GFP striatum, $P = 0.3864$; total brain, $P = 0.1773$; $n = 4$) (Gab/rAAV5-GFP striatum, $P = 0.2626$; total brain, $P = 0.9821$; $n = 4$)). Correlation analysis between MRI volume of enhancement and volume of distribution in the contrast agent/AAV groups showed no statistically significant correlation except for AAV2 Gab when the entire hemisphere was measured (Figure 1, correlation).

For Gab infusions (Figure 1c,d), the volume of contrast enhancement in both striatum and hemisphere tended to be smaller when coinfused with AAV2, while only the striatal volume was smaller with AAV5. Again, these differences were not significant, and differences in total brain volume (*i.e.*, nonstriatal enhancement) may be more related to technical variability in the injection procedure.

Gadoteridol coinfusion results in an increase in the distribution of rAAV5 but not rAAV2 in the rat striatum

To investigate potential effects of gadoteridol (Gd) coinfusion in rAAV distribution efficiency in the striatum, viral preparations of rAAV2 or rAAV5 coding for GFP were coinfused with two different doses of Gd (1 and 2 mmol/l). These doses were chosen because the 1 mmol/l dose has been proposed for use in a clinical trial for Parkinson's disease, whereas 2 mmol/l is the dose commonly used in primate studies.[1,20,34] Coinfusion of viral vector and lactated Ringer's solution were used as controls. Animals were injected bilaterally, and each injection consisted of 1 µl of viral vector and 1 µl of lactated Ringer's solution (left hemisphere) or 1 µl of viral vector and 1 µl of Gd (right hemisphere) (Figure 2a). Quantification of GFP-positive immunostaining was analyzed using densitometry analysis to determine mean optical density (OD), mean area above threshold (AAT), and the ratio of distribution volume (Vd) over infusion volume (Vi). These parameters were calculated using the NIH ImageJ platform (http://rsbweb.nih.gov/ij/index; see Materials and Methods) to define the intensity, area, and volume of transgene expression.

Gd coadministration had a significant effect in the distribution of GFP when rAAV5-GFP was injected (Figure 2a–d). Densitometry analysis of striatal hemispheres showed that the OD of Gd/rAAV5-GFP was 1.5-fold higher relative to the rAAV5-GFP hemisphere at the two doses of Gd (Figure 2a). In addition, the AAT was 2.3-fold and 3-fold higher in the hemispheres with rAAV5-GFP coinjected with 1 and 2 mmol/l Gd, respectively, relative to the hemispheres injected with rAAV5-GFP alone (Figure 2b). The Vd/Vi for rAAV5-GFP was also increased 2.3-fold and 2.9-fold in the presence of 1 and 2 mmol/l Gd, respectively (Figure 2c).

In contrast to the rAAV5 observations, the OD of rAAV2-GFP was unaffected by treatment with Gd. No statistically significant differences in distribution of GFP were found when rAAV2-GFP was coinfused with Gd at the two doses tested (rAAV2-GFP versus 1 mmol/l Gd/rAAV2-GFP, unpaired *t*-test: $P = 0.778$; rAAV2-GFP versus 2 mmol/l Gd/rAAV2-GFP, $P = 0.9414$; Figure 2a). Similarly, the AAT for AAV2-treated striata was unchanged by coinfusion with Gd (rAAV2-GFP versus 1 mmol/l Gd/rAAV2-GFP, unpaired *t*-test: $P = 0.3612$; rAAV2-GFP versus 2 mmol/l Gd/rAAV2-GFP, $P = 0.5904$; Figure 2b). Finally, no significant changes in Vd/Vi were observed in the presence or absence of Gd in the rAAV2-GFP–transduced striata (rAAV2-GFP versus 1 mmol/l Gd/rAAV2-GFP, unpaired *t*-test: $P = 0.3828$; rAAV2-GFP versus 2 mmol/l Gd/rAAV2-GFP, $P = 0.5957$; Figure 2c). In summary, coinfusion of rAAV5-GFP with Gd affected transgene distribution, whereas these properties were unaffected for rAAV2-GFP.

To insure that Gd did not have any adverse effects on tissue health or result in inflammation, three different series of tissue sections were stained for markers of neuroinflammation: Nissl stain (to examine the overall morphology and any possible tissue damage on the injected striata), glial fibrillary acidic protein (GFAP) (a marker for activated astrocytes), and CD-11b (a marker for activated microglia). Nissl staining showed minimal tissue damage around the location of the needle track, which is typical after injections (Figure 2e, left panel). The rest of the tissue had normal morphology irrespective of treatment. GFAP immunostaining revealed minimal active astrocytosis localized to the needle tract in both the lactated Ringer's solution and Gd-injected hemispheres (Figure 2e, middle panel). Similarly, CD-11b staining indicated minimal microglial activation around the needle track, and this was independent of treatment (Figure 2e, right panel).

Gab coinfusion results in an increase in the distribution efficiency of rAAV2 but not rAAV5 in the rat striatum

The distribution differences between rAAV2-GFP and rAAV5-GFP in the Gd coinfusion were unexpected. Next, we investigated the effects of Gab on rAAV distribution in rat striatum. The experimental approach was the same as that in the Gd experiments. In this case, coinfusion of Gab with AAV2 and AAV5 had contrasting effects to those found with Gd coinfusion (Figure 3a). Densitometry analysis of hemispheres coinfused with AAV2 and Gab showed that the mean OD of Gab/rAAV2-GFP was 1.3-fold higher than that of rAAV2-GFP alone (Figure 3b). The AAT was 6.4-fold higher for Gab/rAAV2-GFP than that for rAAV2-GFP alone (Figure 3c). Finally, the Vd/Vi was four times higher in the hemispheres of rAAV2-GFP coinfused with Gab than control vehicle (Figure 3d).

Gab had no effect on the distribution of the rAAV5-GFP vector. We found no differences in the mean OD between the two treatments (Figure 3b; $P = 0.0731$). Similar results were found when analyzing the AAT of AAV5-GFP immunoreactivity (Figure 3c; $P = 0.2236$). Finally, analysis of the Vd/Vi showed a difference between hemispheres coinfused with Gab or vehicle controls. This difference did

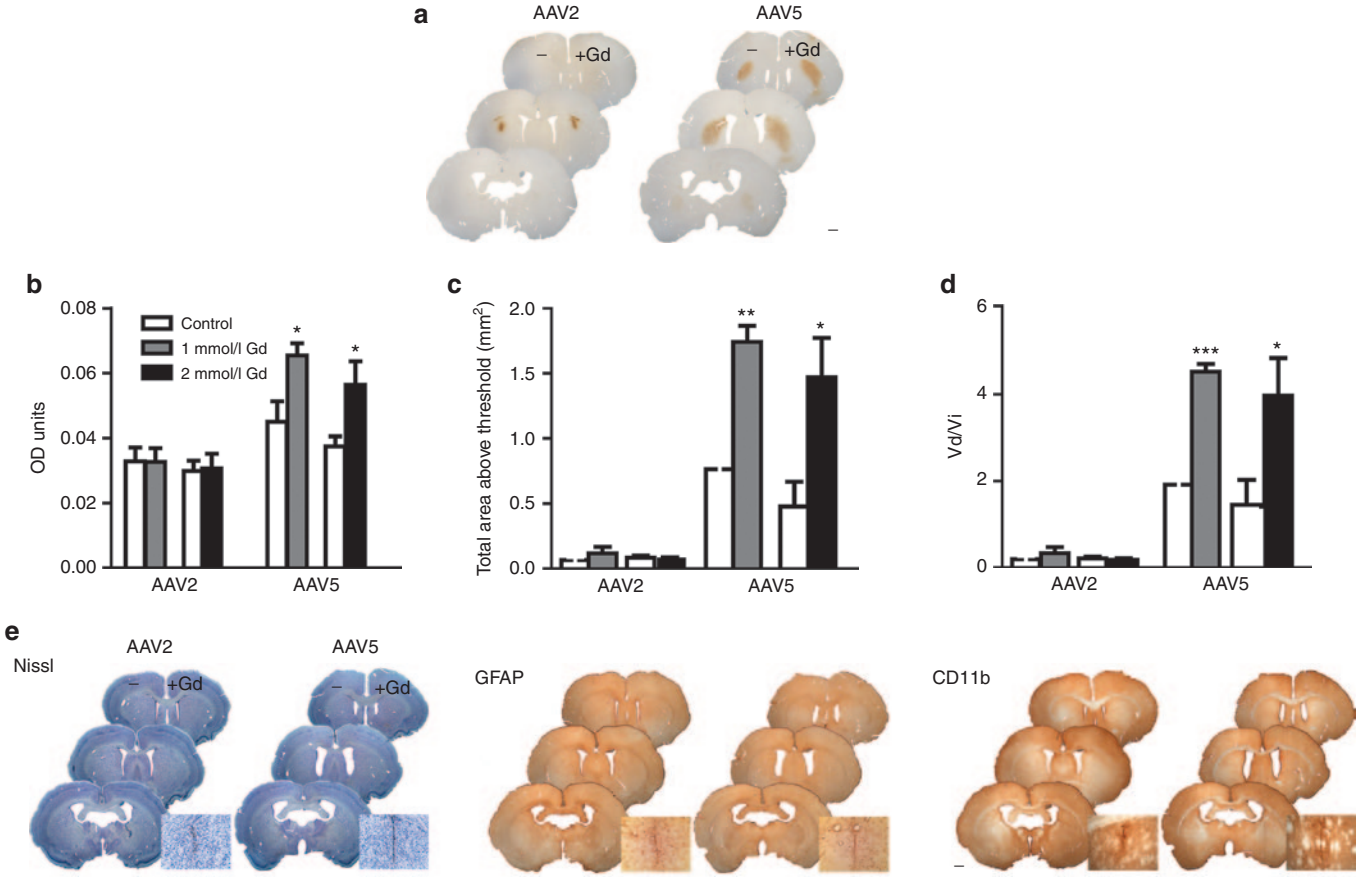

Figure 2 Gadoteridol enhances rAAV5-mediated, but not rAAV2-mediated, distribution in rat striatum. (**a**) Left hemispheres were injected with AAV + lactated Ringer's solution. Right hemispheres were injected with AAV + 2 mmol/l Gd. Similar results were observed with 1 mmol/l Gd (**b–d**). Scale bar = 1 mm. (**b–d**) Quantification of the effects of gadoteridol in the distribution of rAAV2 and rAAV5 by OD analysis. (**b**) Mean OD of GFP immunoreactivity. (**c**) Total area above threshold of GFP immunoreactivity and (**d**) ratio of volume of distribution versus volume of infusion of GFP immunoreactivity (in $mm^3/\mu l$). (**e**) Gadoteridol does not affect tissue health. Left panel: Nissl staining reveals no cell damage outside of the needle track in both hemispheres. Immunostaining for markers of inflammation (middle panel: GFAP, a marker of activated astrocytes; right panel: CD-11b, a marker for activated microglia) show no inflammation in either hemisphere outside of the needle track area. High magnification insets show representative needle track inflammation and cell damage. For all figure panels in **e**, right hemispheres were injected with AAV + Gd and left hemispheres with AAV + lactated Ringer's solution. Scale bar = 1 mm. Data (**a**,**b**,**c**,**d**) represent the mean ± SEM (AAV2 1 mmol/l Gd group, $n = 6$; AAV2 2 mmol/l Gd group, $n = 5$; AAV5 1 mmol/l Gd group, $n = 5$; AAV5 2mmol/l Gd group, $n = 5$). $^*P < 0.05$; $^{**}P < 0.005$; $^{***}P < 0.0005$. Significant indicators above histogram bars indicate comparison to control side (no contrast agent) within same treatment group. Gd, gadoteridol; GFP, green fluorescent protein; OD, optical density; rAAV, recombinant adeno-associated virus.

not reach statistical significance because of the high variability between samples (Figure 3d; $P = 0.303$).

Tissue health in the Gab coinfusion experiments was determined by Nissl staining and immunohistochemistry for GFAP and CD-11b (Figure 3e). Nissl staining did not reveal any cell damage beyond the needle track (Figure 3e, left panel). Gab had no effect on the markers for inflammation, GFAP (Figure 3e, middle panel) or CD-11b (Figure 3e, right panel). These results show that Gab increases distribution efficiency of AAV2 but not AAV5, in stark contrast to the effects of Gd.

Gd does not affect the integrity of either rAAV2-GFP or rAAV5-GFP, while Gab leads to aggregation

To determine if the observed differences in distribution efficiency of rAAV2 and rAAV5 in the presence of the Gd and Gab were due to potential effects of these agents on the integrity and gross morphology of the viral particles, negative-stain EM was used. The capsid morphology of rAAV2-GFP and rAAV5-GFP were unaffected by lactated Ringer's solution as well as incubation with both 1 and 2 mmol/l Gd (Figure 4a–c and Figure 4f–h, respectively). However, pretreatment with 0.1 and 0.2 mmol/l Gab caused the aggregation of the capsid of both viruses (Figure 4d,e (AAV2), Figure 4i,j (AAV5)). The Gab-treated rAAV2-GFP samples appear more sparsely distributed, and the rAAV5-GFP appear aggregated on the negatively stained micrographs when compared with the untreated and Gd-treated samples in all the views observed by EM. There was also an increase in the amount of proteinaceous material in the background of the Gab-treated rAAV2-GFP and rAAV5-GFP particles. These observations suggest that Gab interacts with both the AAV2 and AAV5 capsids and may result in their aggregation.

The rAAV2-GFP and rAAV5-GFP vector genomes show differential sensitivity to Benzonase nuclease treatment in the presence of Gd and Gab

To further corroborate the observations by EM, DNA extraction followed by quantification using real-time PCT (RT-PCR) was conducted for both Gd- and Gab-treated rAAV-GFP samples. The quantities of DNA extracted from rAAV2-GFP in lactated Ringer's solution and pretreated with 1 and 2 mmol/l Gd were not significantly different from each other (Figure 4a). There was, however, ~50% decrease

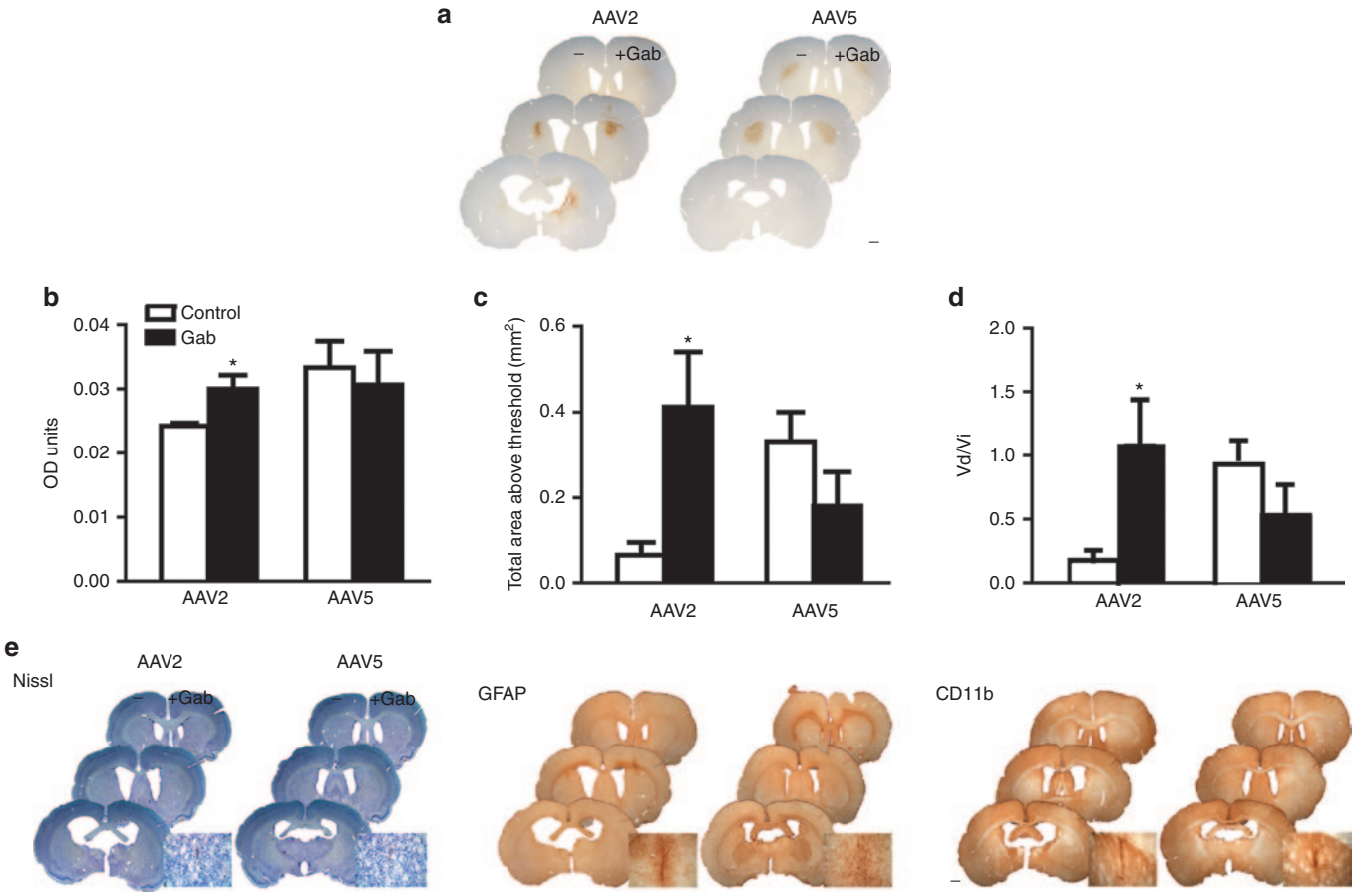

Figure 3 Gab enhances rAAV2 distribution in rat striatum. (**a**) Left hemispheres were injected with AAV + lactated Ringer's solution. Right hemispheres were injected with AAV + 0.1 mmol/l Gab. Scale bar = 1 mm. (**b–d**) Quantification of the effects of Gab in the distribution of rAAV2 and rAAV5 by OD analysis (**b**) Mean OD of GFP immunoreactivity. (**c**) Total area above threshold of GFP immunoreactivity and (**d**) Vd/Vi. (**e**) Galbumin does not affect tissue health. Nissl staining reveals no cell damage outside of the needle track in both hemispheres (left panel). Immunostaining for markers of inflammation (middle panel: GFAP, a marker of activated astrocytes; right panel: CD-11b, a marker for activated microglia) show no inflammation in either hemisphere outside of the needle track area. For all figure panels in **e**, right hemispheres were injected with AAV + Gd and left hemispheres with AAV + lactated Ringer's solution. Insets show representative needle track inflammation and cell damage. Scale bar = 1 mm. Data (**b**,**c**,**d**) represent the mean ± SEM (AAV2 1 mmol/l Gab group, $n = 4$; AAV5 1mmol/l Gab group, $n = 3$). *$P < 0.05$. Significant indicators above histogram bars indicate comparison to control side (no contrast agent) within same treatment group. Gab, galbumin; GFP, green fluorescent protein; OD, optical density; rAAV, recombinant adeno-associated virus.

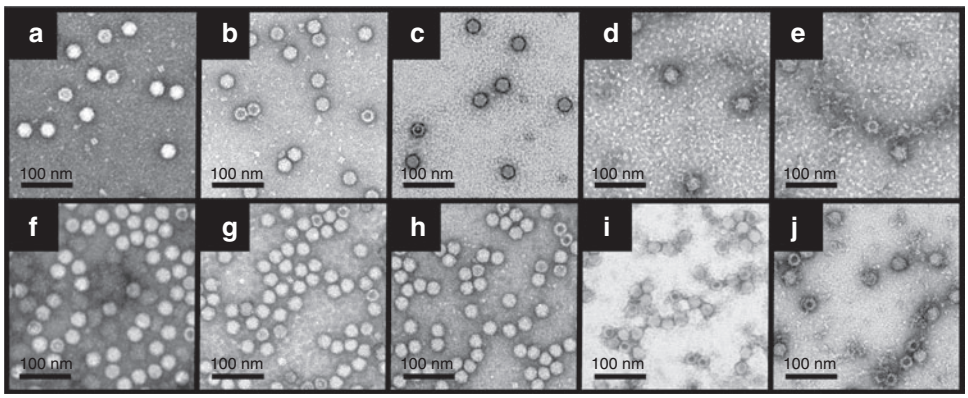

Figure 4 Comparison of the gross morphology of rAAV2-GFP and rAAV5-GFP before and after treatment with Gd and Gab. EMs of rAAV2-GFP in (**a**) lactated Ringer's solution, (**b**) 1 mmol/l Gd, (**c**) 2 mmol/l Gd, (**d**) 0.1 mmol/l Gab, and (**e**) 0.2 mmol/l Gab. The same treatment was repeated for rAAV5-GFPs, and the EMs are shown in (**f**) lactated Ringer's solution, (**g**) 1 mmol/l Gd, (**h**) 2 mmol/l Gd, (**i**) 0.1 mmol/l Gab, and (**j**) 0.2 mmol/l Gab. The scale bar on each figure is 100 nm. EM, electron microscopy; Gab, galbumin; Gd, gadoteridol; GFP, green fluorescent protein; rAAV, recombinant adeno-associated virus.

in genome protection following pretreatment with 1 and 2 mmol/l Gab (Figure 5a). Comparatively, the encapsidated genome in rAAV5-GFP particles were more sensitive to treatment with Gd than the genome packaged within the rAAV2-GFP particles, although the decrease in genome titer was minor at ~15% less than the untreated sample (Figure 5b; one-way ANOVA $P < 0.05$). The genome titers for the Gab-treated rAAV5-GFP vector samples were ~50 and ~15%, respectively, less than the untreated vector, with 0.1 and 0.2 mmol/l Gab incubation. Overall, these observations suggest that Gd may be causing a slight destabilization of rAAV5 that is not observed by EM, and Gab compromises the capsid integrity of both viruses consistent with the visualization by EM.

AAV2 virus-like particles, but not AAV5 virus-like particles, are stabilized by lactated Ringer's solution

Differential scanning calorimetry (DSC) was used to monitor the capsid stability of the AAV2 and AAV5 virus-like particles (VLPs) in the presence of the Gd and Gab contrast agents. This application monitors the transition of macromolecules from native to denatured states and enables the calculation of "melting" temperatures. The melting temperature of AAV2 VLPs in phosphate-buffered saline (PBS) at 67.9 ± 0.2 °C was observed to increase to 75.7 ± 0.7 °C in the presence of lactated Ringer's solution (Table 1 and Figure 6a). AAV2 is slightly further stabilized by treatment with both contrasting agents, with melting temperatures of 77.8 ± 0.6 and 77.3 ± 0.4 °C for treatment with 2 mmol/l Gd and 0.2 mmol/l Gab, respectively (Table 1). Treatment of AAV5 with either lactated Ringer's solution or contrast agents did not affect its stability (Table 1). However, treatment of AAV2 VLPs in PBS with Gd had no effect on the capsid melting temperature (67.5 ± 0.3 and 67.4 ± 0.3 °C, respectively), but a slight decrease in capsid melting was observed for this virus in the presence of PBS and Gab (67.5 ± 0.3 and 66.2 ± 0.3 °C, respectively). The melting temperature for AAV5 VLPs was unaffected in PBS. The observed melting temperature for AAV5 in lactated Ringer's solution is 90.3 ± 0.2 °C, which is 15 °C greater than the melting temperature of AAV2 (Figure 6a,b), and it is approximately the same value obtained for this AAV5 serotype in PBS, which is 89.8 ± 0.3 °C (Table 1). These observations suggest that there may be an ionic component of lactated Ringer's solution, such as Ca^{2+}, or lactate which stabilizes the AAV2 capsid but have no effect on AAV5. This data suggests that AAV2 and AAV5 are aggregating and not disassembling or degrading in the presence of Gab.

DISCUSSION

In this study, we demonstrated that two MRI contrast agents, Gd and Gab, interact differently with the AAV2 and AAV5 serotypes. We selected these two serotypes because AAV2 has been used in most human gene therapy clinical trials, but AAV5 demonstrates a higher distribution of the transgene than AAV2 in the brain (refs.[22–24] and Figures 1 and 2) and thus is a likely candidate serotype for future clinical trials for neurological disorders. First, we showed that Gd enhances the distribution of rAAV5 but not rAAV2, while Gab increased the distribution of rAAV2 but not rAAV5 (Figure 3b–d). The hemispheres coinfused with AAV5 and Gd also showed higher distribution of GFP immunoreactivity in the cortex along the needle track, suggesting a higher backflow of vector in the presence of Gd (Figures 1 and 2a). This is an important fact to consider when evaluating infusion of vectors into the brain and implies that the physics of infusion

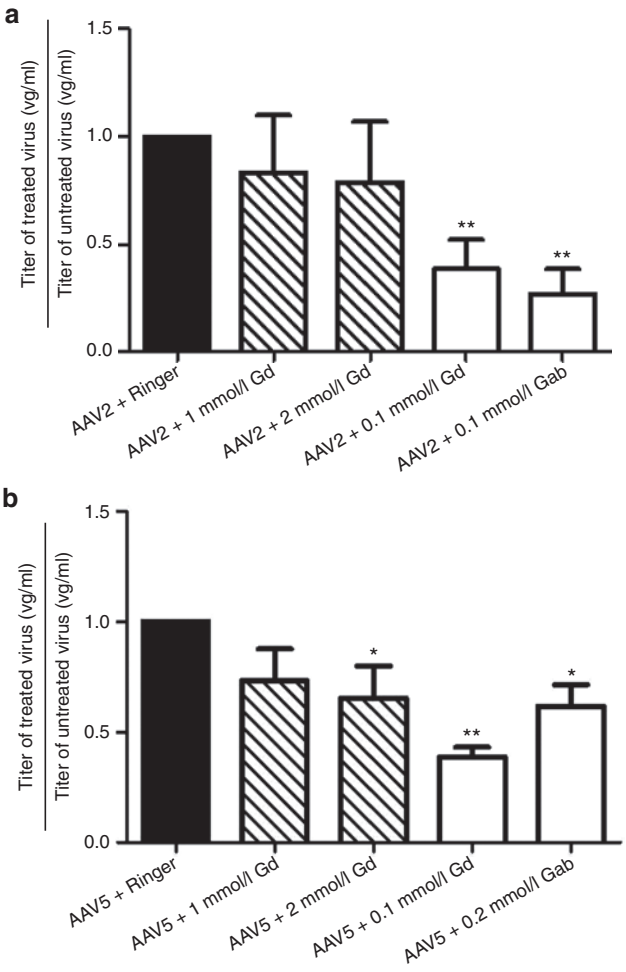

Figure 5 Genome titers for rAAV2-GFP and rAAV5-GFP post-Gd and post-Gab treatment. Histograms comparing the genome titers for (**a**) rAAV2-GFP and (**b**) rAAV5-GFP following packaged genome extraction and quantification by RT-PCR for samples without/with treatment with Gd and Gab. One-way ANOVA analysis was used to determine the statistical significance of the untreated versus treated rAAV2-GFP and rAAV5-GFP samples. *$P < 0.05$ and **$P < 0.001$. AAV, adeno-associated virus; ANOVA, analysis of variance; Gab, galbumin; Gd, gadoteridol; GFP, green fluorescent protein; RT-PCR, real-time PCR.

of viral vectors with MRI contrast agents needs to be optimized for specific combinations of vectors, contrast agents, and brain regions.[35] Note that this investigation does not fully address loss mechanisms associated with delivery parameters (cathether design, flow rate, and schedule) and known issues of infusate loss (backflow, catheter track leakage, perivascular shunting, and overfilling).[1]

The increase in OD and AAT of Gd/rAAV5-GFP were 1.5- and 2.3-fold relative to rAAV5-GFP with no Gd. Although these differences might seem minor, these minor changes in transgene expression levels and distribution could be sufficient to result in major functional changes. Animal studies have demonstrated that small differences (twofold) in the amount of transgene expressed can result in different measureable phenotypes in a dose-dependent manner.[36–39] For example, Richichi *et al*.[40] found that a 1.7-fold difference in the distribution distance of neuropeptide Y in the hippocampus delivered either via rAAV2 (1.5 mm) or the chimeric rAAV1/2 vectors (2.5 mm) resulted in a dose-dependent reduction of kainic acid–induced seizures (50% with AAV2-neuropeptide Y versus 75% with

Table 1 Melting temperatures for AAV2 and AAV5 VLPs treated with Gd and Gab

Treatment	T_m (°C)
AAV2 + PBS	67.53 ± 0.3
AAV2 + PBS + 2 mmol/l Gd	67.4 ± 0
AAV2 + PBS + 0.2 mmol/l Gab	66.2 ± 0.2
AAV2 + lactated Ringer's solution	75.7 ± 0.7
AAV2 + lactated Ringer's solution + 2 mmol/l Gd	77.8 ± 0.6
AAV2 + lactated Ringer's solution + 0.2 mmol/l Gab	77.3 ± 0.4
AAV5 + PBS	89.8 ± 0.1
AAV5 + PBS + 2 mmol/l Gd	89.5 ± 0.4
AAV2 + PBS + 0.2 mmol/l Gab	90.0 ± 0.1
AAV5 + lactated Ringer's solution	90.3 ± 0.2
AAV5 + lactated Ringer's solution + 1mmol/l Gd	90.5 ± 0.1
AAV5 + lactated Ringer's solution + 0.2 mmol/l Gab	90.4 ± 0.2

AAV, adeno-associated virus; Gab, galbumin; Gd, gadoteridol; PBS, phosphate-buffered saline.

AAV1/2). Indeed, low distribution of glial derived neurotrophic factors in the human putamen was attributed as a possible cause for the failure of a phase 2 clinical trial.[41] Increasing the area of distribution of the transgene could be of potential benefit when trying to maximize the area of transgene bioavailability for therapeutic purposes, but it might be deleterious when trying to constrict expression of the therapeutic agent to a specific brain nucleus or region without spillover to other unrelated brain regions.[42–44] These issues should be considered when designing gene therapy experiments in the presence of MRI agents.

We hypothesized that the disparate effects on the two vectors were due to differences in their interaction with Gd and Gab which could have affected their cellular interaction(s) or their capsid integrity and/or stability. Altered receptor binding or uncoating properties could account for the increased distribution observed for the rAAV5-GFP and rAAV2-GFP vectors in the presence of Gd and Gab, respectively. Altered receptor binding might change rAAV vector tropism. We found that this was not the case in a previous report in which we analyzed the effects of Gd on AAV1 and AAV5 distribution in the hippocampus.[35] Materials such as Teflon, steel, and polyimide can result in vector loss due to adsorption of AAV.[45] Therefore, it is possible that Gd in the Gd-AAV solution "coats" the steel needle allowing AAV not to be adsorbed to the metal. On the other hand, this does not explain the selectivity for AAV5 versus AAV2 for Gd or AAV2 versus AAV5 for Gab.

Gadolinium has been shown to modulate fibroblast signaling pathways via platelet-derived growth factor receptor (PDGFR) in cultured fibroblasts and intact skin in organ culture.[46] Activation of these signaling cascades by gadolinium are suppressed by blocking antibodies to the PDGFR, suggesting that gadolinium binds PDGFR. PDGFR is a reported cellular receptor for AAV5,[47] and it is expressed throughout the brain.[48] Therefore, if Gd is binding to PDGFR on the infused cells, this could alter the interaction between this receptor and AAV5, either by reducing affinity or by reducing the number of receptors available for interaction or both. Decreased affinity or receptor numbers could result in increased spread and may account for the higher Vd/Vi observed for the rAAV5-GFP in the presence of this contrast agent. This AAV5 behavior in the presence of Gd would be reminiscent of reports of rAAV2 coinfusion with heparin, which results in an increase in the distribution of the transgene product in the rat striatum. AAV2 and heparin coinfusion might decrease the binding of AAV2 particles

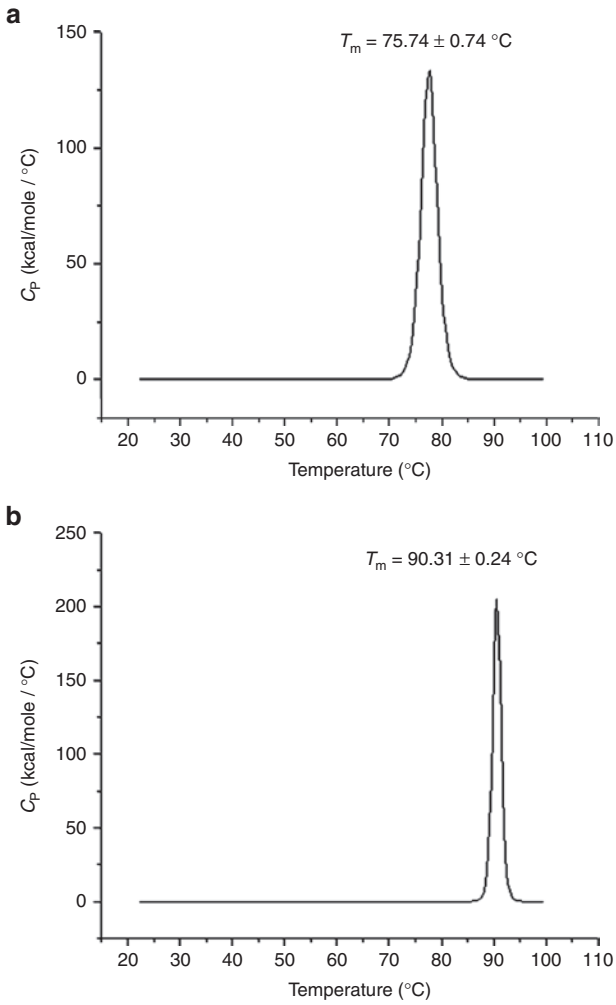

Figure 6 Thermograms for AAV2 and AAV5 VLPs. (**a**) AAV2 and (**b**) AAV5 in the presence of lactated Ringer's solution. The peaks of the thermograms represents the melting temperature of each virus, the melting temperatures of AAV2 and AAV5 are labeled as 75.74 ± 0.74 °C and 90.31 ± 0.24 °C, respectively. AAV, adeno-associated virus.

to cells in the vicinity of the infusion tract by preventing rAAV2 from binding heparin sulfate in the extracellular matrix, which also allows it to move to longer distances before finding a cellular receptor.[49]

AAV2, for which the pattern of distribution appears to be unaffected by treatment with Gd, binds to heparan sulfate proteoglycan as a primary receptor[50] and has been reported to use this interaction for central nervous system transduction.[49] To date, there is no report that would indicate that gadolinium interacts with heparan sulfate proteoglycan and thus interaction with this receptor, abundant in the brain, could be restricting spread. On the other hand, and by analogy to the explanation above, the increased distribution for rAAV2-GFP following coinfusion of Gab could be a result of interaction between the Gab and the heparan sulfate proteoglycan receptor for AAV2 resulting its cell-binding characteristics. It is also possible that the albumin conjugate in Gab interacts with the AAV2 capsid reducing its affinity for heparan sulfate proteoglycan to allow increased spread. The potential for a physical interaction between the Gd and Gab and the AAV vectors in determining the differences in distribution properties of AAV2 and AAV5 were investigated. EM studies showed that the capsid stability of both viruses were

unaffected by the contrast agents. However, Gab is predicted to have resulted in aggregation of both AAV2 and AAV5 capsids rather than degradation due to the visualization of only a few particles per field of view, despite DSC data showing no effect on capsid stability in PBS. The increased stability in lactated Ringer's solution is likely due to components of this buffer and not the contrast agents. Benzonase nuclease sensitivity, of the rAAV2-GFP and rAAV5-GFP vectors, following Gab incubation indicated a decrease in capsid integrity or at least a partial exposure of the packaged genome to nuclease digestion. This would support increased susceptibility to uncoat faster than vector alone without contrast agent. However, calorimetric studies performed on VLPs showed that the composition of the buffer used for viral resuspension in the *in vivo* studies, lactated Ringer's solution, which included the contrast agents, increased stability of AAV2 but had no effect on AAV5 (Figure 5 and Table 1). However, the EM studies did show a change in capsid morphology for AAV2 (Figure 4). Thus, a rearrangement of the capsid is more likely to have occurred to render the encapsulated genome more susceptible to digestion rather than a compromise of capsid integrity in the presence of contrast agent. In addition, in light of the DSC data, it is also possible that the decrease in vector titer, used as an indicator of sensitivity of packaged genome to digestion following contrast agent treatment, is due to interference of the large Gab in the reaction mixture with the Benzonase enzyme. Furthermore, it is also possible that treatment of aggregated samples by the Benzonase enzyme is less effected than untreated or Gd-treated samples and resulted in lower titers. As a note of interest, the observed increase in rAAV2-GFP stability should inform the development of manufacturing methods, since the Ca^{2+} ions or lactate anions contained in lactated Ringer's solution are likely conferring the stable phenotype. Although this attribute is important for sample storage, it may be disadvantageous as a vector since ultimately the particle is required to uncoat to delivery its packaged therapeutic gene.

Based on the fact that AAV5 distribution was enhanced by Gd and AAV2 distribution was enhanced by Gab, we investigated whether the distribution of Gd and Gab were different when coinfused with AAV2 or AAV5 than when injected alone. Our MRI studies showed no significant differences between the Gd-injected side and coinfusion with vector in signal enhancement. The enhancement with Gd was minimal due to the small volume injected and its fast diffusion. In general, it appears that Gd makes AAV5 spread farther and Gab enhances AAV2 distribution (Figures 2a and 3a). Yet, there are no statistically significant differences in the volume of MRI contrast enhancement when Gd or Gab are injected alone or coinfused with viral vector (Figure 1). Moreover, we found no correlation between the volume of contrast enhancement and volume of distribution of the transgene in the striatum (Figure 1). Together, these data suggest that contrast agent distribution does not predict AAV distribution in the striatum. It should be noted that we had a small number of animals (n = 3 or 4), and the volumes injected were small (2 µl; Figures 1–3). Studies in larger animal models might lead to different results. Yet, to our knowledge, nobody has examined the MRI enhancement alone and compared to contrast agent + rAAV in the same study. Our results suggest this needs to be determined empirically for different serotypes and different contrast agents to optimize for clinical studies since MRI contrast agents have been proposed to be used as predictors of viral vector distribution.

In conclusion, this study illustrates that little is known in terms of how these agents interact with viral vectors. The use of contrast agents in targeting of therapeutic vectors can have clinical application. However, the distribution of the MRI contrast agent does not necessarily accurately predict the distribution of the viral vector, though it does provide a ballpark estimate of the spatially affected region. Thus, caution should be applied when interpreting MRI regions of enhancement. Another more significant concern is that the combination of contrast agents and viral vectors result in changes in physical properties of AAV, which may influence the therapeutic outcome. Evaluation of these interactions will be critical when planning clinical trials combining MRI imaging and viral vector delivery. Importantly, this study suggests that alternative technologies to visualize viral vector infusion without the use of MRI contrast agents may be preferential for future human gene therapy clinical trials. Recently, alternative MRI methods have used endogenous contrast mechanisms, relying on changes in T1 due to changes in bulk water content rather than exogenous contrast agents[51] or T2-weighted imaging and diffusion-weighted imaging[52,53] to monitor the infusion distributions, though the relative signal changes are much lower than that for contrast enhanced methods. Continued investigation of quantitative MRI methods may further increase sensitivity to infusion volume without the need for added contrast agents.

MATERIALS AND METHODS

Animal subjects

Sprague Dawley rats were housed in pairs under a 12/12 hour light/dark cycle and given access to food and water *ad libitum*. Protocols were approved by the UW Madison Animal Care and Use Advisory Committee and were in accordance with guidelines established by the US Public Health Policy on Humane Care and Use of Laboratory Animals.

Virus-like particles and viral vectors

Viral preparations for the densitometry, RT-PCR, and EM studies were produced and purified as previously described.[54] Viral vector preparations were buffer exchanged and concentrated as previously described.[54] Viral titers were determined by RT-PCR (rAAV2-GFP = 5×10^{12} vector genomes/ml (vg/ml); rAAV5-GFP = 4.8×10^{12} vg/ml). VLPs for AAV2 and AAV5 were produced using the baculovirus/sf9 expression system and was purified and concentrated to 0.3 mg/ml, as previously described.[55,56] rAAV vectors used for the EM and MRI studies were obtained from the University of Florida Vector Core and had the following titers (estimated by dot blot): rAAV2-GFP = 2.69×10^{12} vg/ml and rAAV5-GFP = 1.24×10^{13} vg/ml.

Intracerebral injections of AAV vectors

All surgical procedures were performed using aseptic techniques and isoflurane gas anesthesia. Bilateral injections were made into the striatum using a stereotaxic frame (Kopf Instruments, Tujunga, CA), and subjects were maintained under isoflurane anesthesia during the injection procedure. Injections were performed with a 10 µl Hamilton syringe fitted with a custom-made beveled 32-gauge needle (Hamilton, Reno, NV). Each injection consisted of a 2 µl reagent volume infused at a rate of 0.5 µl/minute by a Quintissential Stereotaxic Injector (Stoelting, Wood Dale, IL), which allows a precisely controlled rate of injection. The needle was then left in place for 1 additional minute prior to withdrawal from the brain. Coordinates for injection into striatum (AP = 0.0, Lat = ± 3 mm, DV = −4 mm from dura). The right hemisphere received a mixture of either 1 µl Gd or 1 µl Gab and 1 µl viral vector to a final 1 or 2 mmol/l concentration of Gd or 0.1 mmol/l Gab. The left hemisphere received 1 µl viral vector and 1 µl lactated Ringer's solution. Stock solutions of Gd (Prohance; Brako Diagnostics, Princeton, NJ) or Gab (BioPAL, Worcester, MA) were prepared in lactated Ringer's solution: (mEq/l) sodium, 130; potassium, 4; calcium, 2.7; chloride, 109; lactate, 28; and osmolarity, 273 mOsmol/l (pH 6.5) (Baxter Healthcare, Deerfield, IL).The animals included in the MRI portion of the study were also injected bilateraly as follows: The right hemisphere received a mixture of either 1 µl Gd or 1 µl Gab and 1 µl viral vector to a final 2 mmol/l concentration of Gd or 0.1 mmol/l Gab. The left hemisphere received 1 µl Gd or 1 µl Gab and 1 µl lactated Ringer's solution to an equivalent final concentration. Immediately following surgery, MRI data were acquired while animals were under anesthesia. Three weeks after vector injection, animals were sacrificed, and their brains processed for GFP immunohistochemistry.

Tissue processing

Three weeks after vector injection, animals were anesthetized with Beuthanasia-D (150 mg/kg i.p., with supplements if necessary) and perfused through the aorta with a 10 second prewash of PBS (0.01 mol/l phosphate buffer, 137 mmol/l NaCl, pH 7.4) with 0.1% heparin, followed by 500–1,000 ml fixative for 25–30 minutes, packed on ice for 30 minutes to 2 hours, and brain removed into the same fixative. Fixative solutions contained 4% formaldehyde (freshly depolymerized from paraformaldehyde; Sigma, St Louis, MO) in 0.1 mol/l phosphate buffer. Cryoprotection took place in phosphate buffer with 2% dimethyl sulfoxide and a graded series of glycerol concentrations at 4 °C as follows: 10% (1 day), 15% (4 hours), and 20% (4 days). The hemispheres were frozen with dry ice and sectioned in the coronal plane at 45 µm thickness, and sections were transferred to an ethylene glycol–based storage solution and placed in the −20 °C freezer until ready to use. All processing was at room temperature unless otherwise noted.

GFP and Integrin alpha-M (aka: CD-11b, MAC-1, OX-42 antigen) immunohistochemistry: all solutions were prepared with a buffer consisting of PBS with 2% bovine serum albumin (Calbiochem, La Jolla, CA) and 0.1% saponin for GFP or PBS with 0.3% Triton and 0.5% Tween 20 for Integrin alpha-M. Sections for Integrin alpha-M were rinsed followed by a 15-minute incubation in BlokHen (Avēs Labs, Tigard, OR; 1:100). All sections were washed, blocked in buffer with 20% normal serum for 45 minutes, incubated overnight in primary antiserum (GFP from Novus Biologicals, Littleton, CO; 1:30,000 and Integrin alpha-M from Avēs Labs; 1:35) in 1% normal serum. After washes, sections were incubated in 1:300 biotinylated secondary immunoglobulin G (Vector Laboratories, Burlingame, CA) for GFP and 1:1,000 biotinylated secondary immunoglobulin G (Avēs Labs) for Integrin alpha-M for 3 hours, followed by 1 hour in avidin–biotin complex (Standard Elite kit; Vector Laboratories). Final visualization was with 0.04% 3,3′-diaminobenzidine (from tablets; Sigma) and 0.01% H_2O_2 in phosphate buffer (pH 7.4).

GFAP immunocytochemistry

All solutions were prepared with a buffer consisting of PBS with 2% normal serum, 2% lysine, and 0.2% Triton (blocking solution). Sections were washed and incubated overnight in blocking solution at 4 °C. Next day, sections were incubated overnight at 4 °C in primary antiserum (GFAP; DakoCytomation, Carpinteria, CA; 1:5,000). After washes in buffer, the sections were incubated in 1:200 biotinylated secondary immunoglobulin G for 2 hours, followed by 1 hour in avidin–biotin complex (Standard Elite kit; Vector Laboratories). Final visualization was as described above.

Nissl staining

Sections were mounted on subbed slides, dehydrated through graded concentrations of ethanol, cleared with Histo-Clear (National Diagnostics, Atlanta, GA), rehydrated, soaked in cresyl violet stain, dehydrated once again through graded concentrations of ethanol, cleared with Histo-Clear, and coverslipped with Eukitt, Pittsburgh, PA.

Quantification of striatal GFP immunoreactivity

Densitometry analysis was carried out using NIH ImageJ software.[57] Images from 10–12 (30 µm) coronal sections per rat, 0.56 mm apart, were captured using a Nikon E600W microscope equipped with a digital camera (Q Imaging Retiga 2000R; Nikon Instruments, Melville, NY). The threshold for each image was determined using the MaxEntropy function, and the number of particles with an area between 5 and 75 square pixels were recorded. For OD, ImageJ was calibrated using a step tablet, gray scale values were converted to OD units using the Rodbard function, and the area in pixels above a threshold was recorded. Statistical analysis was performed using Prism5 (Graphpad Software, La Jolla, CA) and given as mean ± SEM. Two-tailed, unpaired *t*-tests were performed to determine statistical significance.

Quantitative MRI

Immediately following stereotaxic surgery and infusion, MRI was performed on a 4.7T Varian DirectDrive small animal scanner (Agilent Technologies, Santa Clara, CA) with a quadrature transmit/receive rat head coil built in-house. Mean time from infusion to imaging was 60 minutes for the first infusion and 43 minutes for the second infusioin. Animals were anesthetized using 2% isoflurane delivered via nose cone, positioned using a bite bar and ear bars built into the coil, and monitored for body temperature and respiration rate. The institutional animal care and use committee approved all animal protocols. To assess the volume distribution (V_d) of infusate, quantitative imaging of spin-lattice relaxation time (T_1) was performed using the variable flip angle method,[58] also known as driven equilibrium single-pulse observation of T_1.[59,60] Three-dimensional spoiled gradient echo scans were acquired with TR/TE = 12/5 ms, number of excitations = 8, α = [4 20]° (optimal for T_1 = 1,000 ms),[59] bandwidth = 125 Hz/px, and G_{spoil} = 45 G·ms/cm (strong spoiling regime).[61] The matrix size was 192×192×64 and voxels were 156×156×500 µm³ in volume. Actual flip-angle imaging[62] was performed to measure and correct for inhomogeneous radiofrequency excitation, due to the use of a transmit/receive coil that is small relative to the imaged object. Actual flip-angle imaging parameters were TR_1/TR_2 = 12/60 ms, number of excitations = 4, α = 55°, bandwidth = 376 Hz/px, and G_{spoil} = 45 G·ms/cm (strong spoiling regime). Imaging time was 20:40 minutes per spoiled gradient echo flip angle and 10:27 minutes for actual flip-angle imaging, for a total time of 51:47 minutes.

The acquired images were linearly coregistered, then fitted to Eq. 1 to yield voxelwise estimates of T_1:

$$S_{SPGR} = M_0 \frac{1-E_1}{1-E_1\cos(\alpha)}\sin\alpha \quad \text{with} \quad E_1 = \exp\left(\frac{-\mathrm{TR}}{T_1}\right) \tag{1}$$

Quantitative maps of R_1 (=1/T_1) are linearly proportional to the concentration of contrast agent in that voxel,[63] and quantitative T_1 mapping is more sensitive than commonly performed T_1-weighted imaging, as it removes the confounding effects of receiver coil sensitivity profile, proton density, and inhomogeneous flip angle.[64]

An automatic neural network–based method[65] was used to mask the brain from the rest of the image and estimate total brain volume. A trained expert then manually masked hemisphere, striatal, and infusion volumes, using the automatic mask as a starting point. The volume of infusate was then computed for striatal and nonstriatal volumes. All masks were done using the same window and level settings on the same workstation for consistency across volume estimates.

Mean distribution volumes for the first infusion (60 minutes preimaging) and second infusion (43 minutes preimaging) were compared and found to be 20.22 ± 12.99 µl and 18.99 ± 10.82 µl, respectively, for total enhancement and 10.34 ± 7.95 and µl and 9.09 ± 6.17 µl, respectively, for striatal enhancement, indicating minimal impact on overall volume measurements due to delays between infusion and scanning. The hemisphere infused first was alternated between left and right to further reduce bias.

Visualization of Gd- and Gab-treated rAAV2-GFP and rAAV5-GFP by negative stain EM

To determine the effects of the contrasting agents on the gross morphology of AAV2 and AAV5 particles, the rAAV2-GFP (2.69×10^{12} vg/ml) and rAAV5-GFP (1.24×10^{13} vg/ml) samples were incubated with Gd (1 and 2 mmol/l) and Gab (0.1 and 0.2 mmol/l) in lactated Ringer's solution (Hospira, Lake Forest, IL) for 15 minutes at room temperature. Five microliters of each pretreated sample was loaded onto carbon-coated copper EM grids (Ted Pella, Redding, CA) for 1 minute, washed twice with sterile H_2O, and negatively stained with 5 µl of 2% uranyl acetate for 1 minute. The grids were then air-dried and examined in a FEI Spirit TEM, Hillsboro, OR at a magnification of ×90,000 and accelerating voltage of 120 kV.

Quantitation of rAAV2-GFP and rAAV5-GFP genomes after treatment with Gd and Gab

RT-PCR was used to monitor potential changes in capsid integrity and subsequent genome protection following Gd and Gab treatment. Ten microliters of rAAV2-GFP and rAAV5-GFP vectors were treated with Gd (1 and 2 mmol/l) and Gab (0.1 and 0.2 mmol/l) in lactated Ringer's solution (Hospira) and incubated with 1 µl Benzonase nuclease (Novagen; EMD Chemicals, San Diego, CA) for 1 hour at 37 °C to degrade DNA not encapsidated or protected within the capsid. Each sample was digested with 4 µl proteinase K (Roche, Manheim, Germany) in 20 µl of 10× proteinase K Buffer (10 mmol/l Tris–HCl, pH 8.0, 10 mmol/l ethylenediaminetetraacetic acid, and 10% sodium dodecyl sulfate), and the solution was diluted with sterile distilled H_2O to a total volume of 200 µl. The mixture was incubated for 1 hour in a water bath at 37 °C and extracted twice with an equal volume of phenol chloroform (Roche), with the upper aqueous layer transferred to a clean eppendorf tube after each extraction. Following the second extraction, the aqueous fraction was treated with chloroform (Fisher, Fairlawn, NJ), and the aqueous layer was

transferred to a clean eppendorf. The DNA was precipitated overnight at −20 °C by the addition of 10% NaAc, pH 5.2, 1 µl glycogen, and 3× volume of 95% ethanol. The sample was pelleted by centrifugation at 13,050*g* for 20 minutes at 4 °C. The pellet was air-dried and resuspended with 20 µl water. One microliter of the viral DNA, 1 µl of primers (forward and reverse) to GFP, 12.5 µl of iQ SYBR Green Supermix which contains Taq DNA polymerase (Bio-Rad, Hercules, CA) were combined to a total volume of 25 µl with sterile distilled H_2O. The DNA sample was then run on the Bio-Rad MyiQ system to determine the genome titer.

Differential scanning calorimetry

AAV2 and AAV5 VLPs were dialyzed into PBS (137 mmol/l NaCl, 2.7 mmol/l KCl, 8.1 mmol/l Na_2HPO_4, and 1.47 mmol/l KH_2PO_4, pH 7.4) or lactated Ringer's solution alone and with Gd (2 mmol/l) or Gab (0.2 mmol/l) at 4° C. The final dialysis buffer was used as the reference, and the AAV samples were run at 0.25 mg/ml. The reference and virus samples were loaded in two different chambers of the instrument. The calorimetric assays were conducted in a VP-DSC instrument (MicroCal; GE Healthcare, Pittsburgh, PA), and they were performed by increasing the sample and reference temperature from 20 to 100 °C at a scan rate of 60 °C/hour. The resulting data or thermal scans were plotted and analyzed using the Origin software suite (Origin Lab, Northampton, MA). The thermal scans and melting temperatures of each AAV VLP were obtained in triplicates.

CONFLICT OF INTEREST

The authors declare no conflict of interest.

ACKNOWLEDGMENTS

The authors thank Marina Emborg for invaluable discussions. They also thank Tobias Wood (King's College London) for providing software for automated brain masking. This project was funded by a grant from the Kinetics Foundation to C.B. and a grant R01 AI081961 from the National Institutes of Health to M.A.-M. The authors also thank the rat subjects that participated in this study.

REFERENCES

1 Brady, ML, Raghavan, R, Alexander, A, Kubota, K, Sillay, K and Emborg, ME (2013). Pathways of infusate loss during convection-enhanced delivery into the putamen nucleus. *Stereotact Funct Neurosurg* **91**: 69–78.
2 Kimmelman, J, Duckworth, K, Ramsay, T, Voss, T, Ravina, B and Emborg, ME (2011). Risk of surgical delivery to deep nuclei: a meta-analysis. *Mov Disord* **26**: 1415–1421.
3 Creasy, JL, Price, RR, Presbrey, T, Goins, D, Partain, CL and Kessler, RM (1990). Gadolinium-enhanced MR angiography. *Radiology* **175**: 280–283.
4 Lin, W, Haacke, EM, Smith, AS and Clampitt, ME (1992). Gadolinium-enhanced high-resolution MR angiography with adaptive vessel tracking: preliminary results in the intracranial circulation. *J Magn Reson Imaging* **2**: 277–284.
5 Prince, MR, Yucel, EK, Kaufman, JA, Harrison, DC and Geller, SC (1993). Dynamic gadolinium-enhanced three-dimensional abdominal MR arteriography. *J Magn Reson Imaging* **3**: 877–881.
6 Idée, JM, Port, M, Medina, C, Lancelot, E, Fayoux, E, Ballet, S *et al*. (2008). Possible involvement of gadolinium chelates in the pathophysiology of nephrogenic systemic fibrosis: a critical review. *Toxicology* **248**: 77–88.
7 Sieber, MA, Steger-Hartmann, T, Lengsfeld, P and Pietsch, H (2009). Gadolinium-based contrast agents and NSF: evidence from animal experience. *J Magn Reson Imaging* **30**: 1268–1276.
8 Ding, D, Kanaly, CW, Bigner, DD, Cummings, TJ, Herndon, JE 2nd, Pastan, I *et al*. (2010). Convection-enhanced delivery of free gadolinium with the recombinant immunotoxin MR1-1. *J Neurooncol* **98**: 1–7.
9 Laurent, S, Elst, LV and Muller, RN (2006). Comparative study of the physicochemical properties of six clinical low molecular weight gadolinium contrast agents. *Contrast Media Mol Imaging* **1**: 128–137.
10 Sampson, JH, Brady, M, Raghavan, R, Mehta, AI, Friedman, AH, Reardon, DA *et al*. (2011). Colocalization of gadolinium-diethylene triamine pentaacetic acid with high-molecular-weight molecules after intracerebral convection-enhanced delivery in humans. *Neurosurgery* **69**: 668–676.
11 Sampson, JH, Brady, ML, Petry, NA, Croteau, D, Friedman, AH, Friedman, HS *et al*. (2007). Intracerebral infusate distribution by convection-enhanced delivery in humans with malignant gliomas: descriptive effects of target anatomy and catheter positioning. *Neurosurgery* **60** (2 suppl. 1): ONS89–98; discussion ONS98.
12 Mehta, AI, Choi, BD, Raghavan, R, Brady, M, Friedman, AH, Bigner, DD *et al*. (2011). Imaging of convection enhanced delivery of toxins in humans. *Toxins (Basel)* **3**: 201–206.
13 Nguyen, TT, Pannu, YS, Sung, C, Dedrick, RL, Walbridge, S, Brechbiel, MW *et al*. (2003). Convective distribution of macromolecules in the primate brain demonstrated using computerized tomography and magnetic resonance imaging. *J Neurosurg* **98**: 584–590.
14 Lin, SP and Brown, JJ (2007). MR contrast agents: physical and pharmacologic basics. *J Magn Reson Imaging* **25**: 884–899.
15 Song, DK and Lonser, RR (2008). Convection-enhanced delivery for the treatment of pediatric neurologic disorders. *J Child Neurol* **23**: 1231–1237.
16 Krauze, MT, Mcknight, TR, Yamashita, Y, Bringas, J, Noble, CO, Saito, R *et al*. (2005). Real-time visualization and characterization of liposomal delivery into the monkey brain by magnetic resonance imaging. *Brain Res Brain Res Protoc* **16**: 20–26.
17 Szerlip, NJ, Walbridge, S, Yang, L, Morrison, PF, Degen, JW, Jarrell, ST *et al*. (2007). Real-time imaging of convection-enhanced delivery of viruses and virus-sized particles. *J Neurosurg* **107**: 560–567.
18 Fiandaca, MS, Varenika, V, Eberling, J, McKnight, T, Bringas, J, Pivirotto, P *et al*. (2009). Real-time MR imaging of adeno-associated viral vector delivery to the primate brain. *Neuroimage* **47** (suppl. 2): T27–T35.
19 Su, X, Kells, AP, Salegio, EA, Salegio, EA, Richardson, RM, Hadaczek, P *et al*. (2010). Real-time MR imaging with Gadoteridol predicts distribution of transgenes after convection-enhanced delivery of AAV2 vectors. *Mol Ther* **18**: 1490–1495.
20 Richardson, RM, Kells, AP, Rosenbluth, KH, Salegio, EA, Fiandaca, MS, Larson, PS *et al*. (2011). Interventional MRI-guided putaminal delivery of AAV2-GDNF for a planned clinical trial in Parkinson's disease. *Mol Ther* **19**: 1048–1057.
21 Kim, JH, Astary, GW, Nobrega, TL, Kantorovich, S, Carney, PR, Mareci, TH *et al*. (2012). Dynamic contrast-enhanced MRI of Gd-albumin delivery to the rat hippocampus *in vivo* by convection-enhanced delivery. *J Neurosci Methods* **209**: 62–73.
22 Burger, C, Gorbatyuk, OS, Velardo, MJ, Peden, CS, Williams, P, Zolotukhin, S *et al*. (2004). Recombinant AAV viral vectors pseudotyped with viral capsids from serotypes 1, 2, and 5 display differential efficiency and cell tropism after delivery to different regions of the central nervous system. *Mol Ther* **10**: 302–317.
23 Davidson, BL, Stein, CS, Heth, JA, Martins, I, Kotin, RM, Derksen, TA *et al*. (2000). Recombinant adeno-associated virus type 2, 4, and 5 vectors: transduction of variant cell types and regions in the mammalian central nervous system. *Proc Natl Acad Sci USA* **97**: 3428–3432.
24 Markakis, EA, Vives, KP, Bober, J, Leichtle, S, Leranth, C, Beecham, J *et al*. (2010). Comparative transduction efficiency of AAV vector serotypes 1-6 in the substantia nigra and striatum of the primate brain. *Mol Ther* **18**: 588–593.
25 Mandel, RJ and Burger, C (2004). Clinical trials in neurological disorders using AAV vectors: promises and challenges. *Curr Opin Mol Ther* **6**: 482–490.
26 Mingozzi, F and High, KA (2011). Therapeutic *in vivo* gene transfer for genetic disease using AAV: progress and challenges. *Nat Rev Genet* **12**: 341–355.
27 Simonato, M, Bennett, J, Boulis, NM, Castro, MG, Fink, DJ, Goins, WF *et al*. (2013). Progress in gene therapy for neurological disorders. *Nat Rev Neurol* **9**: 277–291.
28 Bartus, RT, Herzog, CD, Chu, Y, Wilson, A, Brown, L, Siffert, J *et al*. (2011). Bioactivity of AAV2-neurturin gene therapy (CERE-120): differences between Parkinson's disease and nonhuman primate brains. *Mov Disord* **26**: 27–36.
29 Manfredsson, FP and Mandel, RJ (2010). Development of gene therapy for neurological disorders. *Discov Med* **9**: 204–211.
30 Bevan, AK, Duque, S, Foust, KD, Morales, PR, Braun, L, Schmelzer, L *et al*. (2011). Systemic gene delivery in large species for targeting spinal cord, brain, and peripheral tissues for pediatric disorders. *Mol Ther* **19**: 1971–1980.
31 Sherry, AD, Caravan, P and Lenkinski, RE (2009). Primer on gadolinium chemistry. *J Magn Reson Imaging* **30**: 1240–1248.
32 Lauffer, RB, Brady, TJ, Brown, RD 3rd, Baglin, C and Koenig, SH (1986). 1/T1 NMRD profiles of solutions of Mn2+ and Gd3+ protein-chelate conjugates. *Magn Reson Med* **3**: 541–548.
33 Marty, B, Djemaï, B, Robic, C, Port, M, Robert, P, Valette, J *et al*. (2013). Hindered diffusion of MRI contrast agents in rat brain extracellular micro-environment assessed by acquisition of dynamic T1 and T2 maps. *Contrast Media Mol Imaging* **8**: 12–19.
34 Emborg, ME, Joers, V, Fisher, R, Brunner, K, Carter, V, Ross, C *et al*. (2010). Intraoperative intracerebral MRI-guided navigation for accurate targeting in nonhuman primates. *Cell Transplant* **19**: 1587–1597.
35 Hullinger, R, Ugalde, J, Purón-Sierra, L, Osting, S and Burger, C (2013). The MRI contrast agent gadoteridol enhances distribution of rAAV1 in the rat hippocampus. *Gene Ther*.**20**: 1172-1177.
36 Bartus, RT, Brown, L, Wilson, A, Kruegel, B, Siffert, J, Johnson, EM Jr *et al*. (2011). Properly scaled and targeted AAV2-NRTN (neurturin) to the substantia nigra is safe, effective and causes no weight loss: support for nigral targeting in Parkinson's disease. *Neurobiol Dis* **44**: 38–52.
37 Gerstein, H, O'Riordan, K, Osting, S, Schwarz, M and Burger, C (2012). Rescue of synaptic plasticity and spatial learning deficits in the hippocampus of Homer1 knockout mice by recombinant Adeno-associated viral gene delivery of Homer1c. *Neurobiol Learn Mem* **97**: 17–29.
38 Spencer, B, Marr, RA, Rockenstein, E, Crews, L, Adame, A, Potkar, R *et al*. (2008). Long-term neprilysin gene transfer is associated with reduced levels of intracellular Abeta and behavioral improvement in APP transgenic mice. *BMC Neurosci* **9**: 109.
39 Nash, KR, Lee, DC, Hunt, JB Jr, Morganti, JM, Selenica, ML, Moran, P *et al*. (2013). Fractalkine overexpression suppresses tau pathology in a mouse model of tauopathy. *Neurobiol Aging* **34**: 1540–1548.

40 Richichi, C, Lin, EJ, Stefanin, D, Colella, D, Ravizza, T, Grignaschi, G *et al*. (2004). Anticonvulsant and antiepileptogenic effects mediated by adeno-associated virus vector neuropeptide Y expression in the rat hippocampus. *J Neurosci* **24**: 3051–3059.
41 Salvatore, MF, Ai, Y, Fischer, B, Zhang, AM, Grondin, RC, Zhang, Z *et al*. (2006). Point source concentration of GDNF may explain failure of phase II clinical trial. *Exp Neurol* **202**: 497–505.
42 Kordower, JH, Palfi, S, Chen, EY, Ma, SY, Sendera, T, Cochran, EJ *et al*. (1999). Clinicopathological findings following intraventricular glial-derived neurotrophic factor treatment in a patient with Parkinson's disease. *Ann Neurol* **46**: 419–424.
43 Nutt, JG, Burchiel, KJ, Comella, CL, Jankovic, J, Lang, AE, Laws, ER Jr *et al*.; ICV GDNF Study Group. Implanted intracerebroventricular. Glial cell line-derived neurotrophic factor. (2003). Randomized, double-blind trial of glial cell line-derived neurotrophic factor (GDNF) in PD. *Neurology* **60**: 69–73.
44 Eriksdotter Jönhagen, M, Nordberg, A, Amberla, K, Bäckman, L, Ebendal, T, Meyerson, B *et al*. (1998). Intracerebroventricular infusion of nerve growth factor in three patients with Alzheimer's disease. *Dement Geriatr Cogn Disord* **9**: 246–257.
45 Sanftner, LM, Sommer, JM, Suzuki, BM, Smith, PH, Vijay, S, Vargas, JA *et al*. (2005). AAV2-mediated gene delivery to monkey putamen: evaluation of an infusion device and delivery parameters. *Exp Neurol* **194**: 476–483.
46 Bhagavathula, N, Dame, MK, DaSilva, M, Jenkins, W, Aslam, MN, Perone, P *et al*. (2010). Fibroblast response to gadolinium: role for platelet-derived growth factor receptor. *Invest Radiol* **45**: 769–777.
47 Di Pasquale, G, Davidson, BL, Stein, CS, Martins, I, Scudiero, D, Monks, A *et al*. (2003). Identification of PDGFR as a receptor for AAV-5 transduction. *Nat Med* **9**: 1306–1312.
48 Smits, A, Kato, M, Westermark, B, Nistér, M, Heldin, CH and Funa, K (1991). Neurotrophic activity of platelet-derived growth factor (PDGF): rat neuronal cells possess functional PDGF beta-type receptors and respond to PDGF. *Proc Natl Acad Sci USA* **88**: 8159–8163.
49 Nguyen, JB, Sanchez-Pernaute, R, Cunningham, J and Bankiewicz, KS (2001). Convection-enhanced delivery of AAV-2 combined with heparin increases TK gene transfer in the rat brain. *Neuroreport* **12**: 1961–1964.
50 Summerford, C and Samulski, RJ (1998). Membrane-associated heparan sulfate proteoglycan is a receptor for adeno-associated virus type 2 virions. *J Virol* **72**: 1438–1445.
51 Hurley SA, Tromp DPM, Emborg, ME, Ohshima-Hosoyama, S, Brady, M, Raghavan, R, Kubota, K, Alexander, AL *MR Monitoring of Non Contrast-enhanced Brain Infusion with MRI T1 Mapping*. Proceedings of the 20th Annual ISMRM, Melbourne, Victoria, Australia: 2012 p. 48.
52 Richardson, RM, Gimenez, F, Salegio, EA, Su, X, Bringas, J, Berger, MS *et al*. (2011). T2 imaging in monitoring of intraparenchymal real-time convection-enhanced delivery. *Neurosurgery* **69**: 154–163; discussion 163.
53 Iyer, RR, Butman, JA, Walbridge, S, Gai, ND, Heiss, JD and Lonser, RR (2011). Tracking accuracy of T2- and diffusion-weighted magnetic resonance imaging for infusate distribution by convection-enhanced delivery. *J Neurosurg* **115**: 474–480.
54 Zolotukhin, S, Potter, M, Zolotukhin, I, Sakai, Y, Loiler, S, Fraites, TJ Jr *et al*. (2002). Production and purification of serotype 1, 2, and 5 recombinant adeno-associated viral vectors. *Methods* **28**: 158–167.
55 Kohlbrenner, E, Aslanidi, G, Nash, K, Shklyaev, S, Campbell-Thompson, M, Byrne, BJ *et al*. (2005). Successful production of pseudotyped rAAV vectors using a modified baculovirus expression system. *Mol Ther* **12**: 1217–1225.
56 DiMattia, M, Govindasamy, L, Levy, HC, Gurda-Whitaker, B, Kalina, A, Kohlbrenner, E *et al*. (2005). Production, purification, crystallization and preliminary X-ray structural studies of adeno-associated virus serotype 5. *Acta Crystallogr Sect F Struct Biol Cryst Commun* **61** (Pt 10): 917–921.
57 Schneider, CA, Rasband, WS and Eliceiri, KW (2012). NIH Image to ImageJ: 25 years of image analysis. *Nat Methods* **9**: 671–675.
58 Christensen, KA, Grant, DM, Schulman, EM, and Walling, C (1974). Optimal determination of relaxation times of fourier transform nuclear magnetic resonance. Determination of spin-lattice relaxation times in chemically polarized species. *J Phys Chem* **78**: 1971–1977.
59 Deoni, SC, Peters, TM and Rutt, BK (2004). Determination of optimal angles for variable nutation proton magnetic spin-lattice, T1, and spin-spin, T2, relaxation times measurement. *Magn Reson Med* **51**: 194–199.
60 Homer J, Beevers, MS (1985). Driven-equilibrium single-pulse observation of T1 relaxation. A reevaluation of a rapid new method for determining Nmr spin-lattice relaxation times. *J Magn Reson Imaging* **63**: 287–297.
61 Yarnykh, VL (2010). Optimal radiofrequency and gradient spoiling for improved accuracy of T1 and B1 measurements using fast steady-state techniques. *Magn Reson Med* **63**: 1610–1626.
62 Yarnykh, VL (2007). Actual flip-angle imaging in the pulsed steady state: a method for rapid three-dimensional mapping of the transmitted radiofrequency field. *Magn Reson Med* **57**: 192–200.
63 Haar, PJ, Broaddus, WC, Chen, ZJ, Fatouros, PP, Gillies, GT and Corwin, FD (2010). Gd-DTPA T1 relaxivity in brain tissue obtained by convection-enhanced delivery, magnetic resonance imaging and emission spectroscopy. *Phys Med Biol* **55**: 3451–3465.
64 Deoni, SC, Peters, TM and Rutt, BK (2005). High-resolution T1 and T2 mapping of the brain in a clinically acceptable time with DESPOT1 and DESPOT2. *Magn Reson Med* **53**: 237–241.
65 Chou, N, Wu, J, Bai Bingren, J, Qiu, A and Chuang, KH (2011). Robust automatic rodent brain extraction using 3-D pulse-coupled neural networks (PCNN). *IEEE Trans Image Process* **20**: 2554–2564.